Measurement of the decay branching ratios of the α-unbound states in ^{19}Ne and the ^{15}O(α,γ) reaction rate

W. P. Tan,* J. Görres, M. Beard, M. Couder, A. Couture,† S. Falahat, J. L. Fisker, L. Lamm, P. J. LeBlanc, H. Y. Lee,‡ S. O'Brien, A. Palumbo, E. Stech, E. Strandberg, and M. Wiescher

Department of Physics, University of Notre Dame, Notre Dame, Indiana 46556, USA

(Received 23 September 2008; published 14 May 2009)

The breakout reaction ^{15}O$(\alpha,\gamma)^{19}$Ne from the hot CNO cycle is critical to understanding explosive astrophysical phenomena such as x-ray bursts. In spite of considerable past experimental effort via indirect methods, this reaction rate remained mostly uncertain until our recent measurement [Phys. Rev. Lett. **98**, 242503 (2007)] of the eluding α-decay branching ratios of the near-threshold states in ^{19}Ne, particularly the critical level at 4.03 MeV. In this paper, we present more details of and deeper insights into the measurement and the uncertainties of the experimental results. The α-unbound states in ^{19}Ne were populated via the reaction ^{19}F(^{3}He,t), and the α-decay branch was observed from t-α coincidences using a low-energy particle detection array and the TWINSOL facility at the University of Notre Dame. In particular, the measured branching ratio of the 4.03-MeV state is $2.9 \pm 2.1 \times 10^{-4}$. In combination with previous measurements of the lifetimes of these states, a new experimental reaction rate of ^{15}O$(\alpha,\gamma)^{19}$Ne is proposed and discussed in the astrophysical scenario. Further experimental investigations are necessary to reduce the remaining uncertainties.

DOI: 10.1103/PhysRevC.79.055805 PACS number(s): 26.30.Ca, 23.60.+e, 25.55.−e, 27.20.+n

I. INTRODUCTION

X-ray bursts are understood as thermonuclear explosions in the atmosphere of an accreting neutron star in a close binary system [1,2]. The burst conditions are characterized by a sensitive interplay between fuel supply and depletion by nuclear burning. This balance depends critically on the ignition through the nuclear breakout reaction ^{15}O$(\alpha,\gamma)^{19}$Ne, which regulates the flow between the β-limited hot CNO cycle and the rapid proton capture process. When critical values for density and temperature are reached in the neutron star atmosphere, the freshly accreted helium ignites, forming CNO elements via the 3-α reaction, while the accreted hydrogen burns via the hot β-limited CNO cycles at a constant rate [3]. Depending on the strength of the ^{15}O$(\alpha,\gamma)^{19}$Ne reaction, breakout from the hot CNO cycles will occur, fueling the rapid proton capture (rp)-process [4,5] as illustrated in Fig. 1. The rp-process converts the light element fuel into heavy elements from iron and nickel up to cadmium and tin within only a few seconds. This causes a sudden release of nuclear energy of approximately 10^{39-40} ergs [6] in excellent agreement with observation [3–5].

Prior to our study [7], the ^{15}O$(\alpha,\gamma)^{19}$Ne reaction rate was highly uncertain. This prevented using the rate as a tool for identifying the conditions required for the ignition and the recurrence time of the bursts. In fact, sensitivity studies by Fisker *et al.* [8] suggested a theoretical lower limit for the ^{15}O$(\alpha,\gamma)^{19}$Ne reaction rate. On the other hand, Davids *et al.* proposed an experimental upper limit on this reaction rate based on their experimental work [9]. The presently used rate is still mainly relying on theoretical estimates where it has been suggested that the rate is dominated by a single resonance level at an excitation energy of 4.03 MeV in ^{19}Ne [3,10]. While the direct measurement of this resonance is an important goal for radioactive beam facility proposals from the TRIUMF Isotope Separation and Acceleration (ISAC) facility [11] to the future Facility for Rare Isotope Beams (FRIB) [12], the presently available ^{15}O beam intensities are clearly not sufficient for a direct measurement of the resonance strength [13]. Therefore, past efforts have been concentrated on indirect approaches to probe the reaction contributions [9,14–20]. Since the direct capture contribution is negligible [10] over the astrophysical temperature range (0.2–2 GK), the resonances near the α-decay threshold in ^{19}Ne, especially the one at 4.03 MeV, dominate the reaction rate. Thus, we need to obtain the critical resonance parameters to determine reaction rate [21],

$$N_A\langle\sigma v\rangle_{\rm res} \propto (kT)^{-3/2}\Sigma_i(\omega\gamma)_i \exp\left(-\frac{E_i}{kT}\right). \quad (1)$$

The resonance strength is defined as

$$\omega\gamma = \frac{(2J+1)}{2}\frac{\Gamma_\alpha\Gamma_\gamma}{\Gamma_\alpha+\Gamma_\gamma}, \quad (2)$$

where J, E, Γ_α, and Γ_γ represent the spin, energy, and α- and γ-decay widths of each resonance.

Determining the rate indirectly requires measurements of the structural information (spin, excitation energy, Γ_γ, and Γ_α) of the α-unbound states in ^{19}Ne, particularly the ones just above the α-decay threshold. Recently, excitation energies and γ partial widths Γ_γ or lifetimes of the states in ^{19}Ne near the α threshold have been measured with the improved Doppler shift attenuation method at Notre Dame [20]. The result on the lifetime of the 4.03-MeV state and other unbound levels in ^{19}Ne was confirmed in an independent experiment at TRIUMF [22] and a more recently published measurement [23]. The critical quantities to be determined are the corresponding

*wtan@nd.edu
†Present address: Los Alamos National Laboratory.
‡Present address: Argonne National Laboratory.

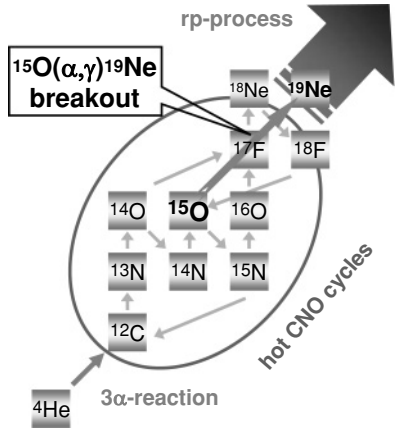

FIG. 1. Nuclear reaction flow by which accreted hydrogen and helium burn into heavier elements. The 3-α reaction converts three helium nuclei into one ^{12}C. The hot-CNO cycle operates at temperatures above 100×10^6 K and converts four hydrogen nuclei into one helium nucleus. The breakout reaction $^{15}O(\alpha,\gamma)^{19}Ne$, which leads into the rp-process, is particularly important for the thermonuclear stability of accreting neutron stars.

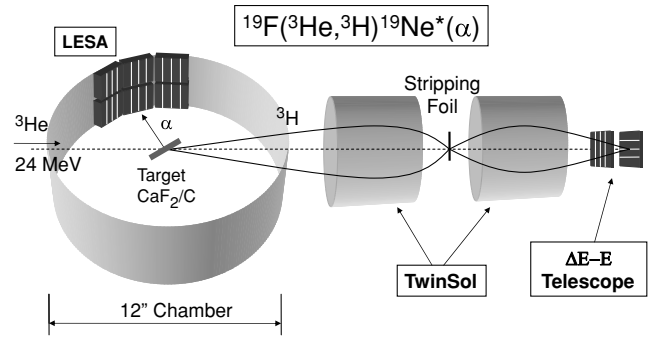

FIG. 2. Schematic setup of this experiment (not to scale for better presentation).

α-decay widths Γ_α or branching ratios $B_\alpha = \Gamma_\alpha/\Gamma$. These parameters have mostly been estimated from the α strengths of the mirror states in ^{19}F with large systematic model-dependent uncertainties inherent to the distorted-wave Born approximation (DWBA) analysis of α-transfer reactions on ^{15}N [10,15,24]. Several attempts have been made in the past to directly measure the relative α-decay widths [9,14,18,25]. While this approach was successful for higher-lying states in ^{19}Ne, it failed for the critical levels near the α threshold due to the low decay branching ratios.

In an abbreviated form of this work [7], we reported the successful laboratory measurement of α-decay branching ratios of the unbound states in ^{19}Ne, in particular of the critical near-threshold states for the first time. More details of the measurement and the analysis are discussed in this paper. Based on this and previous experimental work, we propose an experimental rate for $^{15}O(\alpha,\gamma)^{19}Ne$ that is to replace the more-than-20-year-old theoretical rate [10] and will be suitable for future model studies of astrophysical interest.

II. EXPERIMENTAL SETUP

A number of reactions have been used for populating the excited states in ^{19}Ne and measuring the corresponding α-decay branching ratios. The ^{20}Ne(^{3}He, ^{4}He) reaction in inverse kinematics was studied with the advantage of positive Q value and large cross sections. While the ^{20}Ne(d,t) reaction is handicapped by a small cross section, the ^{21}Ne(p,t) reaction has been used successfully for populating the 4.03-MeV state, as this state is dominated by a five-particle two-hole (5p-2h) intruder configuration [26]. Prior to this work, the two most sensitive attempts for determining B_α of the 4.03-MeV state were done via $p(^{21}\text{Ne},t)$ and ^{3}He(^{20}Ne, ^{4}He) reactions by the Kernfysisch Versneller Instituut (KVI) [9] and Argonne National Laboratory (ANL) [18] groups who reported upper limits of $<4.3 \times 10^{-4}$ and $<6 \times 10^{-4}$, respectively.

Our choice, the (^{3}He, t) reaction, is kinematically favored by its Q value, as in the (^{3}He,^{4}He) case, without the disadvantage of having to use a ^{20}Ne gas target. In contrast to the (p,t) reaction, the (^{3}He, t) reaction preferably populates α-cluster states in ^{19}Ne, which are expected to be favored in the α capture reaction $^{15}O(\alpha,\gamma)$. Therefore we used the ^{19}F(^{3}He, t) reaction to study the α-unbound states in ^{19}Ne and measure their corresponding α-decay branching ratios through the t-α coincidences [7]. One of the main challenges is to obtain large statistics, a demanding task for all the above-mentioned experiments, to reach the sensitivity of 10^{-4} in α-decay branching ratios. Another challenge is the detection of low-energy α particles, which is intrinsic to this experiment. Our approach to overcome these problems will be discussed in the following along with the description of the experimental setup.

A schematic drawing of the experimental setup is shown in Fig. 2. The ^{3}He beam of 24 MeV was produced at the FN tandem accelerator of the University of Notre Dame to bombard a 40-μg/cm^2-thick CaF_2 target that was evaporated on a 20-μg/cm^2 carbon foil. The target was positioned at an angle of 30° with respect to the beam direction to effectively double the target thickness at no expense of more energy loss of low-energy α particles decaying from the ^{19}Ne nuclei. Special target frames/collimators were made with widened horizontal dimensions to compensate for the skews. A segmented Faraday cup at the beam stop were used to fine tune the beam. A beam spot size of about 2mm in diameter was observed during the course of the experiment.

The TwinSol facility at Notre Dame [27], a dual in-line superconducting solenoid ion-optical system originally designed for low-energy radioactive beam studies, was used as a large-acceptance momentum separator to select tritons from other reaction products. Its acceptance range for this experiment was set to $2^\circ \leqslant \theta \leqslant 7.5^\circ$ in polar angles corresponding to a solid angle of 50 msr. To better separate tritons from the elastically scattered ^{3}He with a charge state of +1, a 2.5-μm-thick Mylar foil was placed in between the two solenoids to strip the additional electron from ^{3}He. A large-area multistrip ΔE-E telescope was positioned close to the focal plane of TwinSol to identify and track tritons. It consists of two 500-μm-thick silicon-pad detectors (5×5 cm^2) that are segmented into four pads each to form a 16-pixel telescope. Tritons were identified

using the ΔE-E technique as well as measured on energy and timing. The triton position information was used for kinematic corrections, which will be discussed in the next section.

A low-energy silicon-strip array (LESA) was designed and constructed to detect the low-energy α particles from the decay of the excited states in ^{19}Ne above the α-decay threshold [7]. The array consists of six identical 300-μm-thick silicon-pad detectors, each of which has four pads and a size of 4×4 cm^2. LESA was positioned 8 cm away from the target, covering a solid angle of about 10% of 4π for $60^\circ \leqslant \theta \leqslant 150^\circ$ in the laboratory frame. To reduce the detection threshold, the front dead layer of the silicon detectors was limited to a thickness of <0.05 μm, which translates into an energy loss of <14 keV for 200-keV α particles. The size of the chamber that houses LESA is minimized to about 30 cm in diameter to fully utilize the acceptance capacity of TwinSol. The particle identification was achieved by measuring the particle's energy and time of flight from the target to LESA, since the energy of relevant α particles can be well below 1 MeV.

III. DATA ANALYSIS

In Fig. 3, the ΔE-E particle identification technique is demonstrated for the particles detected in the focal plane telescope. The big blob in the lower left part of the figure comprises the high-energy deuterons from the (^{3}He, d) reaction, which obviously has much higher cross sections. These deuterons punched through both layers of the silicon detectors. The smaller blob just below the gated area shows the tritons from the (^{3}He, t) reaction via the ground state of ^{19}Ne, which have energy high enough to punch through the telescope as well.

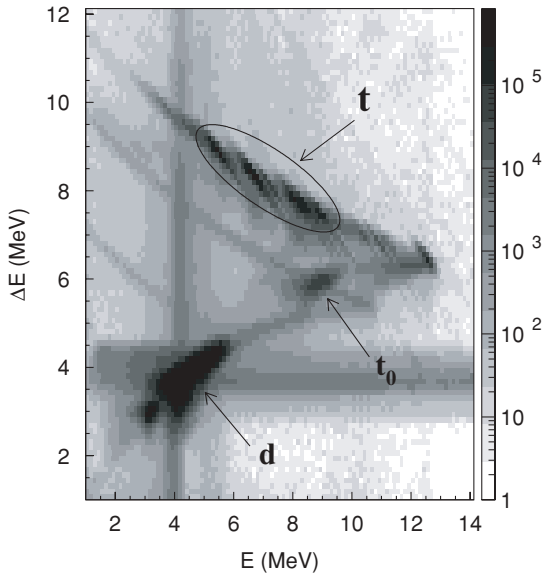

FIG. 3. Two-dimensional ΔE-E plot for particle identifications in the telescope. The tritons related to the α-unbound states in ^{19}Ne are denoted by t, while high-energy tritons corresponding to the ground state of ^{19}Ne and deuterons from the (^{3}He, d) reaction that punched through both detectors of the telescope are labeled with t_0 and d, respectively.

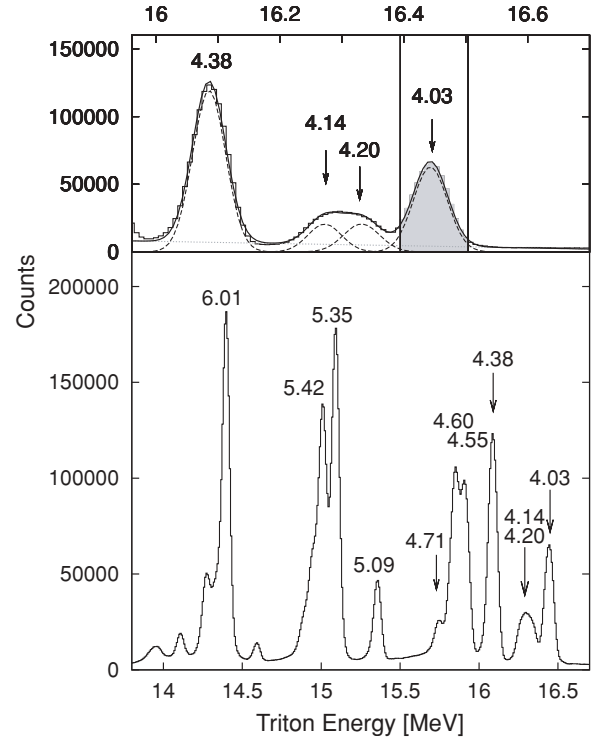

FIG. 4. Total energy spectrum of tritons detected in the telescope corresponding to the triton gate of the α-unbound states in ^{19}Ne, as illustrated in Fig. 3. Peaks related to the excited states in ^{19}Ne are labeled. The region of the states at 4.03–4.38 MeV is enlarged in the top panel where we fit the peaks with Gaussian functions, and the shaded area shows the gate of the 4.03-MeV state.

The gated area demonstrates the tritons with a striped pattern populating the individual excited states in ^{19}Ne, where the length of these stripes shows the nonuniformity of thickness in the ΔE detector. The gated tritons were then projected to the axis of total energy, and the resulting one-dimensional triton energy spectrum is shown in Fig. 4. The α-unbound states in ^{19}Ne are well observed for excitation energies of 4–6 MeV. An exception is the 4.63-MeV $13/2^+$ state, which has little contribution due to its high spin. Thus, gates on individual states (except the unresolved $7/2^-$ and $9/2^-$ states at energies of 4.14 and 4.20 MeV) could be set to study the α-decay channels in coincidence. In particular, the important 4.03-MeV state is reasonably well separated from the other states. Fitting the peaks with Gaussian functions (as shown in the top panel of Fig. 4) shows that the 4.14-MeV state overlaps with the gate of the 4.03-MeV state by less than 1%, while the 4.20-MeV state has essentially no contribution to the 4.03-MeV gate. The effect on the branching ratio of the 4.03-MeV state is negligible compared to the large statistical uncertainty of α decays, which will be discussed later.

Furthermore, enough counts were collected to ensure that the sensitivity of the measurements of α-decay branching ratios reaches as low as 10^{-4}. However, double hits in the telescope inevitably contribute to the background in the triton spectrum in Fig. 3. In rare cases, double-hit events with high-energy electrons can contaminate a given triton peak with tritons from higher-lying states (at least 0.5 MeV higher in

energy) [7]. The effect on small α-decay branching ratios is demonstrated below.

The energy spread of α particles detected in LESA is dominated by the angular resolution of LESA and the tracking uncertainties of tritons. Significant kinematic shifts of α energy were observed with regard to the position on the telescope where tritons are detected. To reduce the kinematic energy spread, a correction using the triton tracking information was applied. The kinematic effect of the triton detection on α energy is shown in Fig. 5, where the α energy spectra from a typical detector pad of LESA for the 5.35-MeV state are plotted before and after the kinematic corrections are applied.

For low-energy particles, the time of flight (TOF) varies significantly with the kinetic energy as stated by the relation $t \propto 1/\sqrt{E}$, where the TOF increases dramatically for energy below 500 keV. To better examine the TOF signal, a flattening algorithm was applied to correct the energy dependence of the TOF so that one-dimensional gates on the TOF would be better applied for low-energy α particles. Figure 6 shows the kinematically corrected TOF spectra for the resonances of interest. The position of the timing gate for α particles (indicated by the shaded area) is obvious for the states above 4.55 MeV with large α-decay branching ratios. For the states at 4.03–4.38 MeV with weak α-decay signals, the same timing gate is ensured by the kinematic corrections. A peak on the left of the gate for these lower-lying states was created by fast coincident electrons. These electrons were produced from Compton scattering and pair production of the dominating γ-ray decays in these levels.

In Fig. 7, the α energy spectra in LESA are plotted after the above-mentioned corrections in coincidence with tritons gated for the 4.55–5.09 MeV states. The total α spectra are presented in the left panels, while the net spectra are plotted in the right panels after subtracting the background. For these higher-lying states, the α-decay signals are quite pronounced,

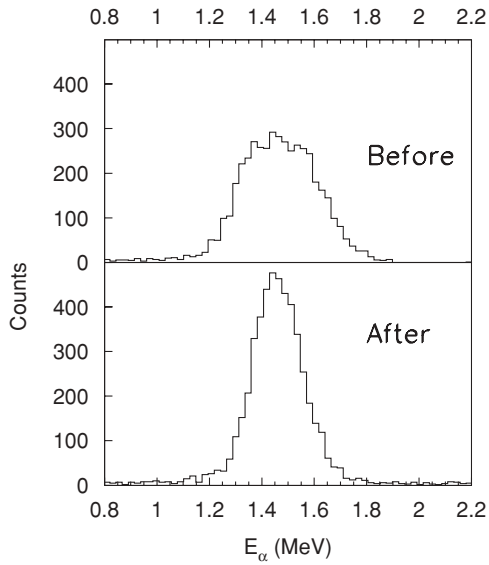

FIG. 5. α energy spectra for the 5.35-MeV state are compared before and after the kinematic corrections are applied.

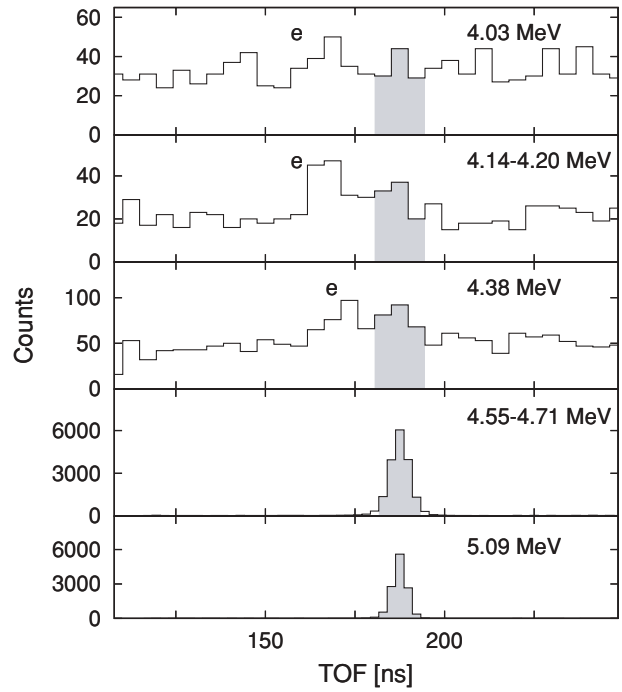

FIG. 6. Kinematically corrected TOF spectra for the states at 4.03–5.09 MeV. The shaded areas demonstrate the timing gates of the corresponding αs which were applied to obtain the α energy spectra in Figs. 7 and 8. For the states at 4.03–4.38 MeV with weak α decays, a peak on the left of the gate was created by coincident electrons. See text for details.

making it easy to extract the corresponding decay branching ratios.

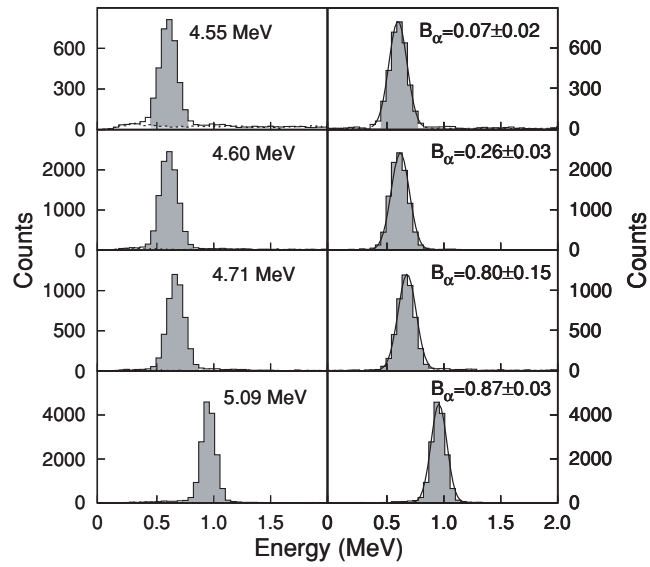

FIG. 7. Kinematically corrected α energy spectra in coincidence with the tritons for the higher-lying α-unbound states at 4.5–5.09 MeV. Left panels: total spectra. Right panels: net coincident events after subtracting the background. Shaded areas present the expected α energy range for the corresponding states in ^{19}Ne, and the smooth curves are simulated calculations assuming a decay branching as measured.

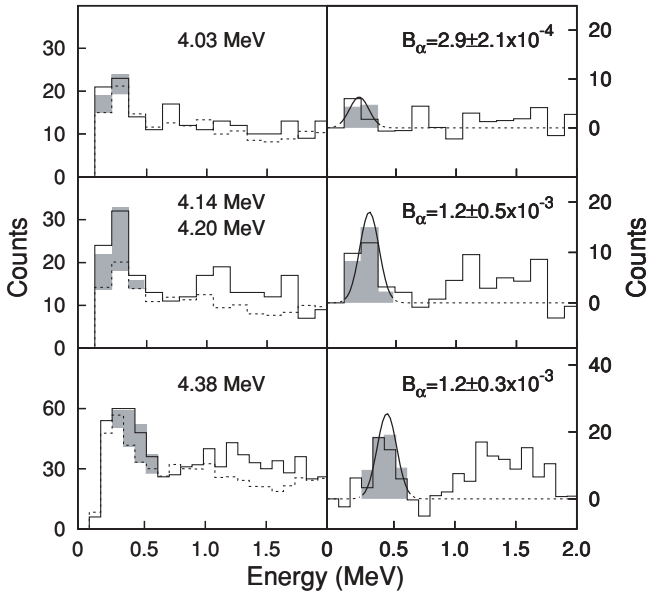

FIG. 8. Coincident α energy spectra for the lower-lying α-unbound states at 4.03–4.38 MeV. Left panels: total α-decay events (solid histograms) and the background (dashed histograms). Right panels: net spectra after the background deduction. Note that these histograms are NOT corrected in kinematics. For comparison, the shaded areas present the kinematically corrected net events as shown in Fig. 3 of Ref. [7]. The smooth curves are simulated calculations assuming a decay branching as measured. The net events at higher energies (i.e., above the shaded areas) are α particles decaying from higher-lying states ($\geqslant$4.55 MeV) with much larger B_α that leak into the triton gates of the lower-lying states. See text for details.

However, very weak α-decay branching ratios on the order of 10^{-3} or less were observed for the levels near the α-decay threshold. In Fig. 8, the coincident α particles within corresponding triton gates for lower-lying states at 4.03–4.38 MeV are plotted before (left panels) and after (right panels) the background deduction. The background was obtained from random coincidence events outside the α timing gates which have a much larger count rate than those within the gates for the rare α-decay cases. For this reason, the additional statistical error from the determination of the background does not contribute significantly to the uncertainty of the net spectra.

Note that Fig. 8 is presented differently from Fig. 3 in Ref. [7] for clarification. The difference is mainly that kinematically corrected coincident events are only shown in the expected α energy range (shaded areas) relevant to their corresponding levels, while uncorrected spectra (histograms) are depicted throughout the plots in Fig. 8. In such a way, we can remove misleading artifacts at energies unrelated to the gated levels introduced by kinematic corrections. However, additional structures at higher energies are also noticeable for these low decay branching states. These structures are identified as α-decay events leaking from higher-lying states with much larger B_α because of double-hit events with high-energy electrons. Electron hits around 0° are common in experimental devices such as the dual solenoid system used in our experiment. Because of the detector thickness of our telescope, the electrons have an energy loss of at least 0.5 MeV. An electron will likely deposit more energy if it enters the detector at an angle. This happens especially in the E detector, as electrons are likely scattered at large angles when passing through the ΔE detector. A contaminating level at an excitation energy higher by 0.5 MeV corresponds to tritons with energy lower by 0.5 MeV. So it will affect the triton gate of interest when an electron hit coincides with an α-decay event in the higher energy region in Fig. 8. It is obvious that the level needs to be at least 0.5 MeV higher to contribute, while the contribution will be smaller as the level is farther from the level of interest, since it will be harder to leak into the gate drawn in the ΔE-E particle identification plot. For this reason, the levels at 4.55–4.71 MeV do not contaminate the spectra of the 4.14–4.38 MeV states but may contribute slightly to the 4.03-MeV level spectrum, while the levels above 5 MeV contribute more and more as seen in the spectra from the 4.03–4.38 MeV states. Fortunately, the resulting 0.5-MeV gap is sufficient to separate these αs from the weak α-decay signals for the states at 4.03–4.38 MeV.

To obtain the α-decay branching ratios, we need to determine the detection efficiencies of the coincident α particles. The $1/2^+$ state at 5.35 MeV decays almost 100% via the α channel and yields an isotropic distribution of emitted α particles [14]. Thus the α-decay yields of other states can be normalized to that of the 5.35-MeV state, and their angular correlation with tritons close to 0° can be parametrized as [28]

$$w(\theta) = \sum_{M,m} p_M \left| \left\langle \frac{1}{2} m; l(M-m) \middle| JM \right\rangle Y_{lM-m}(\theta, \phi) \right|^2, \quad (3)$$

where the $\langle \frac{1}{2} m; l(M-m) \mid JM \rangle$ are the Clebsch-Gordan coefficients that couple the spin of $1/2^-$ ^{15}O and the orbital angular momentum l of the spinless α to the spin J of an excited state in ^{19}Ne, the Y_{lM-m} are the spherical harmonics, and the p_M are the populations of substate M. Such distributions are symmetric about 90° in the center-of-mass frame and easy to obtain for the higher-lying states at 4.55–5.09 MeV, as shown in Fig. 9, because of relatively large α-decay branchings. The fitted distributions in Fig. 9 were then integrated over the 4π solid angle for the total number of decaying α particles. The α-decay branching ratio of a given excited state can therefore be determined from the ratio of the number of α particles to the number of corresponding tritons after being normalized to that of the 5.35-MeV state.

Unfortunately, limited statistics due to the weak α decays prohibit similar analysis for the 4.03–4.38 MeV states. Note that the α-decay angular distributions of the 4.55–5.09 MeV states in Fig. 9 are relatively flat because of large acceptance of TwinSol for triton detection. Alternatively, the total number of α particles can be estimated by counting the number of α particles in the backward detectors of LESA (between 90° and 150° in the laboratory frame, roughly 100°–155° in the center-of-mass frame) while assuming an isotropic angular distribution. We found that there is little difference (less than 5%) between the total numbers of α particles obtained from this simple approach and from the fitting of the angular distribution. Therefore we can obtain the branching ratios of the lower-lying states without the knowledge of angular distributions. As seen in Fig. 8, the main uncertainties of the

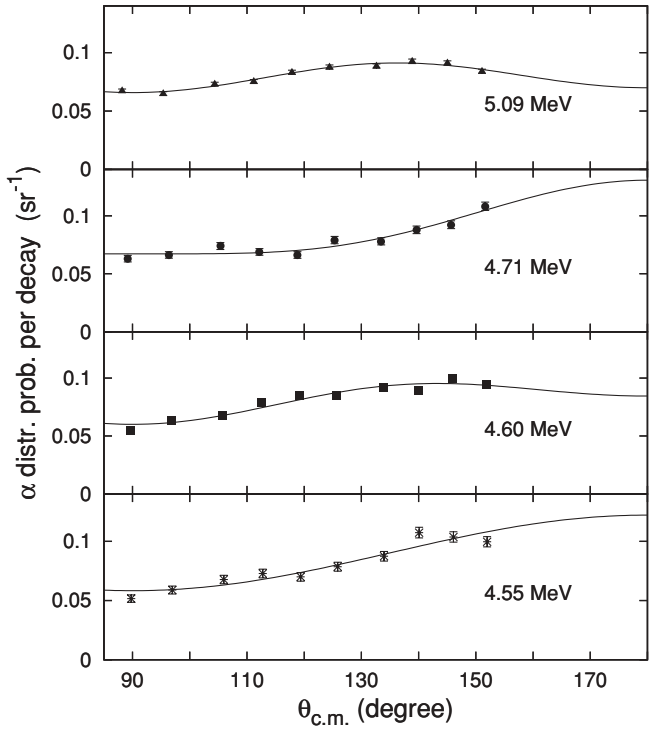

FIG. 9. α-decay angular distributions for the 4.55–5.09 MeV states with significant α-decay branchings. The fitted curves were obtained by assuming a correlation described in Eq. (3).

α-decay branching ratios for the lower-lying states come from the low statistics.

IV. α-DECAY BRANCHING RATIOS

Table I shows our new branching ratio results in comparison with previous measurements where one-sigma errors are presented. For the critical 4.03–4.38 MeV states near the threshold, there are no previous results available besides the upper limit constraints (for the values of the 4.38-MeV state from Refs. [14,18], see discussion below). Our work presents for the first time experimental values for these states on the one-sigma level. In particular, an α-decay branching ratio of 2.9×10^{-4} with one-sigma error of 2.1×10^{-4} was measured for the 4.03-MeV state, which is critical to determining the $^{15}O(\alpha,\gamma)$ reaction rate. The result is consistent with the previous 90% C.L. upper limits of $<4.3 \times 10^{-4}$ [9] and $<6 \times 10^{-4}$ [18]. Note that net α-decay events, at the level of 1.4σ statistical significance, were observed in this experiment in contrast to previous measurements. Assuming that all the observed counts are from background in the spirit of a null measurement, we would set an upper limit of 3.9×10^{-4} at 90% C.L. from our measurement using the Bayesian approach (as applied in previous results). For the astrophysics discussions below, we adopt our measured branching ratio within the one-sigma error.

The two states at 4.14 and 4.20 MeV could not be resolved, but a combined branching ratio of $1.2 \pm 0.5 \times 10^{-3}$ was determined. On the one hand, the measured α peak in Fig. 8 seems to be lower in energy than the simulated one, indicating that these decay events are more likely from the 4.14-MeV state. On the other hand, spectroscopic factor estimates seem to favor the 4.20-MeV state. To obtain the spectroscopic factor, we have calculated the single-particle α width using a Woods-Saxon potential with a radius parameter of $r_0 = 1.36$ fm and a diffuseness of $a = 0.7$ fm. If all the coincidences would result from the decay of the 4.14-MeV state, the resulting spectroscopic factor would be 1 to 4, taking into account the experimental uncertainties of the branching and the lifetime. However, assuming that all the coincidences result from the decay of the upper level at 4.20 MeV, we arrive at a spectroscopic factor of $0.45^{+0.35}_{-0.25}$, a value expected from predictions [10]. However, such calculations are model dependent and simply carry too much uncertainty to make a conclusion on this issue. For example, using a different parameter set ($r_0 = 1.4$ fm, $a = 0.6$ fm) adopted by Fortune [30] in the above calculation, the derived spectroscopic factor will be about 1.7 times larger. A further experimental investigation of the doublet is therefore needed.

The branching ratio of the 4.14 and 4.20 MeV doublet is surprisingly large compared to previous predictions and assessments [10,18]. They have long been ignored in the past in calculating the reaction rate because of the previously anticipated small branching ratios. As seen in Fig. 10 and Sec. VI, however, their contribution to the rate is far from negligible and could be dominant at some temperatures. Such an unexpected contribution may suggest a possible α-cluster

TABLE I. Measured α-decay branching ratios of the states at 4.03–5.09 MeV in ^{19}Ne compared with the previous results. The weighted average values are adopted for calculating the $^{15}O(\alpha,\gamma)$ rate. See text for detailed discussion.

E_x (MeV)	4.03	4.14 & 4.20	4.38	4.55	4.60	4.71	5.09
Ref. [14]			0.044 ± 0.032	0.07 ± 0.03	0.25 ± 0.04	0.82 ± 0.15	0.90 ± 0.09
Ref. [29]	<0.03		<0.04	$0.09^{+0.04}_{-0.02}$	$0.29^{+0.06}_{-0.04}$	$0.67^{+0.23}_{-0.14}$	$1.11^{+0.17}_{-0.13}$
Ref. [17]	<0.01	<0.01		0.32 ± 0.03 (3 levels combined)			1.8 ± 0.9
Ref. [18]	$<6 \times 10^{-4}$		$16 \pm 5 \times 10^{-3}$				0.8 ± 0.1
Ref. [9]	$<4.3 \times 10^{-4}$		$<3.9 \times 10^{-3}$	0.16 ± 0.04	0.32 ± 0.04	0.85 ± 0.04	0.90 ± 0.06
Ref. [19]			(>0.0027) tentative	0.06 ± 0.04	0.208 ± 0.026	$0.69^{+0.11}_{-0.14}$	$0.75^{+0.06}_{-0.07}$
This work	$2.9 \pm 2.1 \times 10^{-4}$	$1.2 \pm 0.5 \times 10^{-3}$	$1.2 \pm 0.3 \times 10^{-3}$	0.07 ± 0.02	0.26 ± 0.03	0.80 ± 0.15	0.87 ± 0.03
Adopted	$2.9 \pm 2.1 \times 10^{-4}$	$1.2 \pm 0.5 \times 10^{-3}$	$1.2 \pm 0.3 \times 10^{-3}$	0.08 ± 0.02	0.26 ± 0.02	0.83 ± 0.04	0.86 ± 0.03

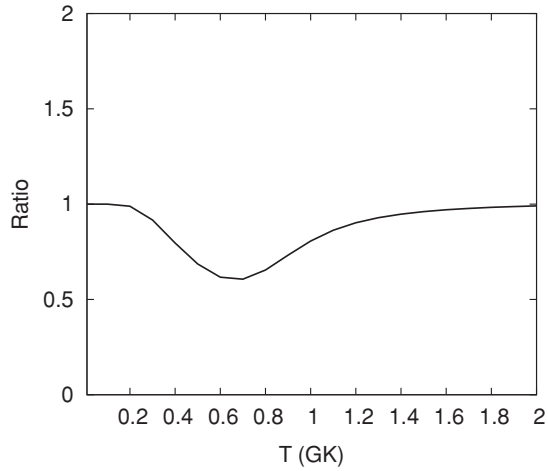

FIG. 10. Ratio of the $^{15}O(\alpha,\gamma)^{19}Ne$ reaction rate assuming that the 4.20-MeV state dominates the α decay over the 4.14-MeV state to the rate that favors the 4.14-MeV state domination. See text for details.

configuration. In Ref. [9], no α decay was observed from the two states, because the (p,t) reaction does not favor the population of α-cluster states, and the combined yield of these two states is over 20 times lower than that of the 4.03-MeV state in their experiment [9]. On the other hand, the $(^3He,t)$ reaction we chose tends to populate more α-cluster states, and these two states have comparable yield to the 4.03-MeV state, thus making a measurement of the α decay possible.

As for the 4.38-MeV state, the present result of $1.2 \pm 0.3 \times 10^{-3}$ agrees with the stringent upper limit of $<3.9 \times 10^{-3}$ [9], while it differs from previously given values of 0.044 ± 0.032 [14] and $16 \pm 5 \times 10^{-3}$ [18]. In Ref. [14], the value for the 4.38-MeV state was clouded by lack of statistics, as no peak was seen in the timing spectrum. On the other hand, the experiment in Ref. [18] could not resolve the relevant states in ^{19}Ne, and the poor resolution allowed contamination from other states with much larger B_α to overwhelm the possible decay from the 4.38-MeV state.

For the states at higher excitation energies of 4.55–5.09 MeV with large α-decay branching ratios, our new measurements are in good agreement with previous results [9,14,17–19,29]. The error bars for the 4.55-, 4.60-, and 4.71-MeV states stem mainly from the uncertainty in separating them in triton spectra (see Fig. 4). The 4.64-MeV state could not be identified, but it is a high-spin $(13/2^+)$ state with a negligible α-decay branching ratio on the order of 10^{-5} [10].

V. ISOSPIN SYMMETRY

The experimental work via the reaction of $^{17}O(^3He, n\text{-}\gamma)$ [20] has not only given first results on lifetimes of the α-unbound states in ^{19}Ne but also resulted in more accurate energy and spin values. In Table II, the results are shown along

TABLE II. Measured values of lifetimes [20,22] and α-decay widths of the α-unbound states in ^{19}Ne are compared with the corresponding values of the mirror states in ^{19}F from the literature. The adopted resonance strengths are mostly based on the experimental information of τ_m and B_α. Note that the Γ_α^{exp} and $\omega\gamma$ values of the 4.14–4.20 MeV doublet are shown for two extreme cases (see Sec. IV) and should not be used at the same time. See text for discussion.

^{19}Ne ([20] and this work)					^{19}F [31]		$\Gamma_\alpha^{calc}(^{19}Ne)$ (meV)
E_x (keV)	J^π	τ_m (fs)	Γ_α^{exp} (meV)	$\omega\gamma$ (meV)	τ_m (fs)	Γ_α (meV)	
4034.5 ± 0.8	$\frac{3}{2}^+$	13^{+9}_{-6}	0.017 ± 0.013	0.033 ± 0.026	9 ± 5		0.011 [15]
		11^{+4}_{-3} [22]					
4143.5 ± 0.6	$\frac{7}{2}^-$ [a]	18^{+2}_{-3}	0.044 ± 0.020	0.18 ± 0.08	19 ± 7		
4200.3 ± 1.1	$\frac{9}{2}^-$ [a]	43^{+12}_{-9}	0.018 ± 0.009	0.09 ± 0.04	67 ± 15		
4377.8 ± 0.6	$\frac{7}{2}^+$	5^{+3}_{-2}	$0.16^{+0.11}_{-0.07}$	$0.63^{+0.45}_{-0.28}$	<11	$1.5^{+1.5}_{-0.8} \times 10^{-6}$ [24]	0.18
						$3.6 \pm 1.2 \times 10^{-6}$ [32]	0.44
4547.7 ± 1.0	$\frac{3}{2}^-$	15^{+11}_{-5}	$3.5^{+2.0}_{-1.7}$	$6.5^{+3.5}_{-3.1}$	17^{+10}_{-8}	$3.2 \pm 1.3 \times 10^{-3}$ [33]	2.5
4601.8 ± 0.8	$\frac{5}{2}^+$	7^{+5}_{-4}	24^{+33}_{-10}	54^{+72}_{-23}	6.5 ± 3.5 [34]	$3.2 \pm 0.4 \times 10^{-2}$ [33]	84
						1.6×10^{-2} [24]	42
						$3.2 \pm 0.7 \times 10^{-2}$ [35]	84
						$6.2 \pm 1.2 \times 10^{-2}$ [32]	160
4634.0 ± 0.9	$\frac{13}{2}^+$	$>1 \times 10^3$		3.15×10^{-5} [10]	$3.7 \pm 0.4 \times 10^3$		
4712 ± 10	$\frac{5}{2}^-$		200 ± 70	101 ± 21	15.4 ± 3.0	1.9 ± 0.2 [33]	390
						2.1 ± 0.7 [36]	430
						3.0 [24]	620
5092 ± 6	$\frac{5}{2}^+$			14 ± 4		3.3 ± 0.6 [33]	34
						4.5 ± 2.7 [37,38]	48

[a]Previous spin assignments [31,39] were the other way around (see text).

with a recent measurement for the 4.03-MeV state [22]. We also recognize a new publication on these lifetimes [23], which are not included in the following reaction rate calculations. An interesting comparison with the measured lifetimes of analog states in ^{19}F is also presented in Table II. The similar lifetime values for both ^{19}Ne and ^{19}F support the previous assumptions of mirror symmetry [10]. By comparing the decay scheme of the states in ^{19}Ne to that of the mirror states in ^{19}F with well-assigned spin values, we can confirm or improve on most of the spin assignments in ^{19}Ne. In particular, for the 4.14- and 4.20-MeV states, we found out that the previous tentative spin assignments should have been exchanged as shown in Table II. It is important, as we will see the significance of these two states in the discussion of the reaction rate below.

Similarly, comparisons of the α-decay widths are shown in Table II. The α-decay widths $\Gamma_\alpha^{\rm exp}$ for ^{19}Ne are derived from the measured lifetimes in this table and the α-decay branching ratios in Table I, except for the 4.71-MeV state where the γ width is taken from a value of 40.7 ± 8.1 meV measured for the mirror state in ^{19}F [36]. Such an assumption for the 4.71-MeV state is well justified from the similar lifetime values of other states for ^{19}Ne and ^{19}F. Based on the experimental information of lifetimes and α-decay widths, the resonance strengths $\omega\gamma$ were calculated using Eq. (2) and are listed in Table II. Included are the states up to 4.71 MeV in ^{19}Ne, where one-sigma error bars are calculated assuming that the errors in B_α and τ are independent. The values listed for the two states at 4.14–4.20 MeV are obtained assuming that the α decays are solely from either of them and therefore represent two extreme cases, as discussed in Sec. IV.

As for the 5.09-MeV state, the required experimental information is not complete, and we have to resort to the mirror symmetry to obtain an $\omega\gamma$ for this ^{19}Ne state. The α widths for ^{19}F from various references in Table II are deduced mainly from resonance strengths measured for ^{19}F in consideration of nearly 100% γ-decay branchings [38] whereupon we can calculate the corresponding α widths $\Gamma_\alpha^{\rm calc}$ for ^{19}Ne (rightmost column in Table II) as follows:

$$\Gamma_\alpha^{\rm calc}(^{19}{\rm Ne}) = \Gamma_\alpha(^{19}{\rm F})\frac{\Gamma_\alpha^{\rm sp}(^{19}{\rm Ne})}{\Gamma_\alpha^{\rm sp}(^{19}{\rm F})}. \quad (4)$$

Here the single-particle widths $\Gamma_\alpha^{\rm sp}$ take into account the Coulomb barrier difference of the two systems of $^{15}{\rm O}+\alpha$ and $^{15}{\rm N}+\alpha$ and can be calculated by [21]

$$\Gamma_\alpha^{\rm sp} = \frac{2\hbar}{R}\left(\frac{2E}{\mu}\right)^{1/2}\frac{1}{F_l^2+G_l^2}, \quad (5)$$

where E and μ are the center-of-mass energy and the reduced mass, respectively, and F_l and G_l are the regular and irregular Coulomb wave functions, respectively. The nuclear interaction radius R is assumed to be 5 fm for both ^{15}O-α and ^{15}N-α systems. As a matter of fact, the ratio of the two $\Gamma^{\rm sp}$ is very insensitive to R and varies only a few percent for a range of radii between 3 and 7 fm. Similar values within a factor of 2 between the calculated α widths for ^{19}Ne (rightmost column) and the experimental values (fourth column) in Table II, again, show that good isospin symmetry is justified for the two nuclei of ^{19}Ne and ^{19}F. The resulting $\omega\gamma$ for the 5.09-MeV state is obtained using the α width calculated from the mirror state [33] and the experimental α-decay branching ratio in Table I.

TABLE III. Resonance parameters of the states between 5.3 and 6.5 MeV taken mainly from the mirror ^{19}F [31] for calculating the $^{15}{\rm O}(\alpha,\gamma)^{19}{\rm Ne}$ rate.

E_x (^{19}F) (keV)	$E_{\rm x}$(^{19}Ne) (keV)	J^π	$\omega\gamma$ (eV) [31,33]
5337 ± 2	5351 ± 10	$\frac{1}{2}^+$	1.67 ± 0.11
5418 ± 1		$\frac{7}{2}^-$	0.388 ± 0.040
5463.5 ± 1.5	5424 ± 7	$\frac{7}{2}^+$	2.14 ± 0.13
5500.7 ± 1.7	5463 ± 20	$\frac{3}{2}^+$	3.62 ± 0.32
5535 ± 2	5539 ± 9	$\frac{5}{2}^+$	0.360 ± 0.038
5621 ± 1		$\frac{5}{2}^-$	0.330 ± 0.035
5938 ± 1	5832 ± 9	$\frac{1}{2}^+$	0.430 ± 0.045
6070 ± 1	6078 ± 6 [40]	$\frac{7}{2}^+$	2.21 ± 0.23
6088 ± 1	6016 ± 6 [40]	$\frac{3}{2}^-$	4.8 ± 0.5
6100 ± 2	6107 ± 6 [40]	$\frac{9}{2}^-$	0.440 ± 0.069
6160.6 ± 0.9	6138 ± 6 [40]	$\frac{7}{2}^-$	2.4 ± 0.6
6255 ± 1		$\frac{1}{2}^+$	0.35 [10]
6282 ± 1	6290 ± 6 [40]	$\frac{5}{2}^+$	1.0 ± 0.2
6330 ± 2		$\frac{7}{2}^+$	0.76 ± 0.15
6429 ± 8	6437 ± 9	$\frac{1}{2}^-$	0.1 [10]
6496.7 ± 1.4	6419 ± 6 [40]	$\frac{3}{2}^+$	1.7 ± 0.3
6500.0 ± 0.9		$\frac{11}{2}^+$	2.3 ± 0.4
6527.5 ± 1.4	6450 ± 6 [40]	$\frac{3}{2}^+$	2.4 ± 0.4

To complete the calculation of the $^{15}{\rm O}(\alpha,\gamma)^{19}{\rm Ne}$ reaction rate over the astrophysical relevant temperature range, we incorporate also the contributions from the higher-lying states up to around the proton threshold. These contributions may significantly influence the rate at higher temperatures. Very little experimental information is available for the ^{19}Ne states between 5.3 and 6.5 MeV. Their resonance strengths as well as some spin and energy values have to be obtained from the mirror states in ^{19}F. Fortunately, all these states are dominated by α decay for both ^{19}Ne and ^{19}F, making $\omega\gamma \simeq \omega\Gamma_\gamma$ a good approximation. Therefore the resonance strengths for ^{19}Ne is about the same as those for ^{19}F, as the good mirror symmetry is ensured by the lifetime values shown in Table II. The resonance strength values for these states taken from the average of the measured values for ^{19}F [31,33], or otherwise from the theoretical estimate [10], are adopted in Table III, where the energy and spin values are taken from ^{19}Ne [31,40] if available and from ^{19}F otherwise [31].

VI. EXPERIMENTAL RATE OF $^{15}{\rm O}(\alpha,\gamma)^{19}{\rm NE}$

Based on our new measurements of α-decay branching ratios and recent experiments on lifetimes [20,22] for the α-unbound states in ^{19}Ne, we can obtain, for the first time, an experimental rate of the $^{15}{\rm O}(\alpha,\gamma)$ breakout reaction at temperatures of astrophysical interest based on Eq. (1). The adopted level information and the corresponding resonance

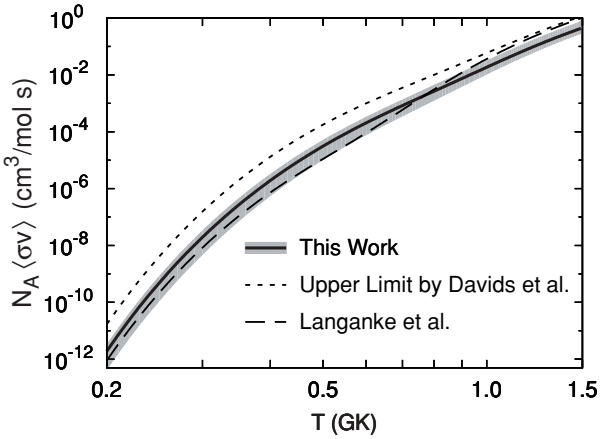

FIG. 11. New resonant $^{15}O(\alpha,\gamma)$ reaction rate (solid line) for the states at 4.03–5.09 MeV, with one-sigma uncertainty indicated by the shaded area. Previous upper limit (dotted line) by Davids *et al.* [9] and a widely adopted theoretical rate (dashed line) by Langanke *et al.* [10] are also shown for comparison.

strengths are shown in Tables I–III for calculating the $^{15}O(\alpha,\gamma)$ reaction rate. To demonstrate the possible large effects from the two unresolved 4.14–4.20 MeV states, we assign the α-decay branching solely to the 4.14-MeV state for calculating the rate.

Figure 11 shows the reaction rate using the new level information, where one-sigma uncertainty is depicted by the grey area. For comparison, only contributions from the states at 4.03–5.09 MeV are considered in the plots as they dominate the rate at astrophysically relevant temperatures. The previous upper limit of the reaction rate (dotted line) is taken from the work of Davids *et al.* [9] who combined their upper limit of B_α for the 4.03-MeV state with the γ width limit obtained by Hackman *et al.* with the Coulomb excitation approach [16]. Also presented in Fig. 11 is the theoretical estimate of the rate by Langanke *et al.* [10], which has long been adopted for simulation studies of various astrophysical models. Our new measurement confirms that the estimate for the overall rate is reasonably accurate. However, the contributions from individual resonances shown in Fig. 12 are dramatically changed compared to the prediction of Langanke *et al.* In particular, if the 4.14-MeV state has a nonvanishing α-decay branching ratio (see discussions in Sec. IV), it may contribute significantly to the rate throughout the breakout process and even dominate the rate at $0.7 < T_9 < 0.9$. This has been mostly ignored in the past. At peak temperatures (1–2 GK) of an x-ray burst, it is actually the 4.60-MeV state that dominates the rate instead of the 4.55-MeV state as calculated by the Langanke rate. Similar results on the 4.55–4.60 MeV states were obtained using the information from the mirror states in ^{19}F [9]. Here we draw this conclusion solely from experiments on α-decay branching ratios and lifetimes [20] of ^{19}Ne.

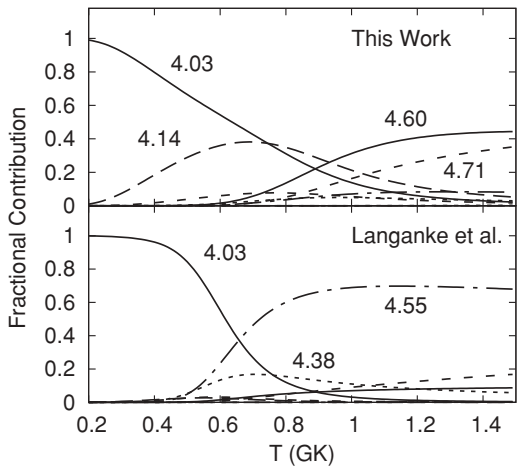

FIG. 12. Fractional contributions from the individual states in ^{19}Ne to the $^{15}O(\alpha,\gamma)$ reaction rate for this work (upper panel) assuming that the 4.14-MeV state dominates the α decay over the 4.20-MeV state and the widely used estimate of Langanke *et al.* [10] (lower panel).

Table IV shows the tabulated values of the rate for a wide temperature range of 0.01–10 GK. The rate takes into account direct capture contributions [41] below 0.2 GK, which are significant at $T < 0.1$ GK and contributions from higher-lying states up to the proton threshold, which are important at extreme temperatures. The uncertainties are estimated where such information is available. The rates are provided for a wide temperature range to be suitable for model studies. The rates for the range $0.1 < T_9 < 2$ which have impact on the here discussed x-ray burst scenario are mostly based on our new experimental results (i.e., the tabulated rates in this range are very similar to the resonant rate of the 4.03–5.09 MeV states presented in Fig. 11).

TABLE IV. Values of the $^{15}O(\alpha,\gamma)^{19}Ne$ rate at $0.01 < T < 10$ GK are calculated from the level information of all the α-unbound states in ^{19}Ne up to the proton threshold in Tables I–III and the direct capture contributions [41] up to 0.2 GK.

T_9	$N_A\langle\sigma v\rangle$ (cm^3/mol s)		
	Mean	Low	High
0.01	9.31×10^{-68}	–	–
0.02	1.68×10^{-51}	–	–
0.04	1.22×10^{-38}	–	–
0.06	2.11×10^{-32}	–	–
0.08	1.80×10^{-28}	–	–
0.1	1.09×10^{-24}	3.20×10^{-25}	1.87×10^{-24}
0.2	1.89×10^{-12}	4.08×10^{-13}	3.38×10^{-12}
0.3	1.94×10^{-8}	4.64×10^{-9}	3.42×10^{-8}
0.4	1.93×10^{-6}	5.44×10^{-7}	3.32×10^{-6}
0.5	3.11×10^{-5}	1.02×10^{-5}	5.21×10^{-5}
0.6	2.04×10^{-4}	7.56×10^{-5}	3.37×10^{-4}
0.7	8.36×10^{-4}	3.46×10^{-4}	1.38×10^{-3}
0.8	2.67×10^{-3}	1.23×10^{-3}	4.47×10^{-3}
0.9	7.43×10^{-3}	3.80×10^{-3}	1.27×10^{-2}
1	1.87×10^{-2}	1.03×10^{-2}	3.27×10^{-2}
1.5	0.507	0.339	0.863
2	3.78	2.86	5.65
4	168	148	196
6	640	568	723
8	1.17×10^3	1.03×10^3	1.31×10^3
10	1.59×10^3	1.40×10^3	1.78×10^3

VII. ASTROPHYSICAL IMPLICATIONS AND CONCLUSIONS

The impact of the new $^{15}O(\alpha,\gamma)^{19}Ne$ rate on x-ray bursts has been extensively investigated [7,42] in the framework of a dynamical and self-consistent spherically symmetric x-ray burst model [8]. For detailed discussions, refer to the papers by Tan *et al.* [7] and Fisker *et al.* [42]. The important findings are summarized as follows.

The uncertainties of the new rate are significantly reduced compared to previous estimates [8]. This allows not only a better identification of the ignition conditions of x-ray bursts but also the improved analysis of the dynamics and mechanism of x-ray bursts. In this context, the accretion rate corresponding to the transition point between steady state and unstable burning is of particular interest. Calculations for a range of accretion rates were performed for the new reaction rate. The accretion rate at the transition point was determined to be $\dot{M} \geqslant 2.0 \times 10^{18}$ g/s with much improved uncertainty of $<10\%$ compared to previous uncertainties of one order of magnitude [8].

The burning process on accreting neutron stars depends not only on the $^{15}O(\alpha,\gamma)^{19}Ne$ rate but also significantly on the accretion rate, the composition of the accreted matter, the surface gravity of the neutron star, and other individual reaction rates (e.g., the 3α rate), forming a complex feedback cycle. Better constraint on the $^{15}O(\alpha,\gamma)^{19}Ne$ rate will hopefully reduce the complexity of the problem and invigorate other parameter studies in this process. However, the experimental error on the α-decay branching ratio of the 4.03-MeV state is still uncomfortably large, and further experimental work is needed for better determining the $^{15}O(\alpha,\gamma)^{19}Ne$ rate.

These calculations demonstrate the importance of the laboratory results for providing stringent limits for the burning conditions in stellar objects. It demonstrates how experimental nuclear data can complement observational results and provide important insights for astrophysical model simulations. The $^{15}O(\alpha,\gamma)^{19}Ne$ reaction is the key to our understanding of the onset of x-ray bursts. The experimental results bring us closer to a better understanding of the complex interplay between fuel supply and burning processes at the extreme conditions of the neutron star atmosphere.

ACKNOWLEDGMENTS

This work has been supported by the National Science Foundation under Grant No. PHY01-40324 and the Joint Institute for Nuclear Astrophysics, NSF-PFC under Grant No. PHY02-16783.

[1] S. E. Woosley and R. E. Taam, Nature (London) **263**, 101 (1976).
[2] P. C. Joss, Nature (London) **270**, 310 (1977).
[3] M. Wiescher, J. Görres, and H. Schatz, J. Phys. G **25**, R133 (1999).
[4] R. Wallace and S. Woosley, Astrophys. J. Suppl. Ser. **45**, 389 (1981).
[5] H. Schatz, A. Aprahamian, J. Görres, M. Wiescher, T. Rauscher, J. Rembges, F.-K. Thielemann, B. Pfeiffer, P. Möller, K.-L. Kratz *et al.*, Phys. Rep. **294**, 167 (1998).
[6] S. E. Woosley, A. Heger, A. Cumming, R. D. Hoffman, J. Pruet, T. Rauscher, J. L. Fisker, H. Schatz, B. A. Brown, and M. Wiescher, Astrophys. J. Suppl. Ser. **151**, 75 (2004).
[7] W. P. Tan, J. L. Fisker, J. Görres, M. Couder, and M. Wiescher, Phys. Rev. Lett. **98**, 242503 (2007).
[8] J. L. Fisker, J. Görres, M. Wiescher, and B. Davids, Astrophys. J. **650**, 332 (2006).
[9] B. Davids, A. M. van den Berg, P. Dendooven, F. Fleurot, M. Hunyadi, M. A. de Huu, R. H. Siemssen, H. W. Wilschut, H. J. Wörtche, M. Hernanz *et al.*, Phys. Rev. C **67**, 065808 (2003).
[10] K. Langanke, M. Wiescher, W. Fowler, and J. Görres, Astrophys. J. **301**, 629 (1986).
[11] D. A. Hutcheon, S. Bishop, L. Buchmann, M. L. Chatterjee, A. A. Chen, J. M. D'Auria, S. Engel, D. Gigliotti, U. Greife, D. Hunter *et al.*, Nucl. Instrum. Methods A **498**, 190 (2003).
[12] Report of the Rare Isotope Science Assessment Committee, 2006, http://www7.nationalacademies.org/bpa/RISAC.html.
[13] F. Vanderbist, P. Leleux, C. Angulo, E. Casarejos, M. Couder, M. Loiselet, G. Ryckewaert, P. Descouvemont, M. Aliotta, T. Davinson *et al.*, Eur. Phys. J. A **27**, 183 (2006).
[14] P. V. Magnus, M. S. Smith, A. J. Howard, P. D. Parker, A. E. Champagne *et al.*, Nucl. Phys. **A506**, 332 (1990).
[15] Z. Q. Mao, H. T. Fortune, and A. G. Lacaze, Phys. Rev. Lett. **74**, 3760 (1995).
[16] G. Hackman, S. M. Austin, T. Glasmacher, T. Aumann, B. A. Brown, R. W. Ibbotson, K. Miller, B. Pritychenko, L. A. Riley, B. Roeder *et al.*, Phys. Rev. C **61**, 052801(R) (2000).
[17] A. M. Laird, S. Cherubini, A. N. Ostrowski, M. Aliotta, T. Davinson, A. D. Pietro, P. Figuera, W. Galster, J. S. Graulich, D. Groombridge *et al.*, Phys. Rev. C **66**, 048801 (2002).
[18] K. E. Rehm, A. H. Wuosmaa, C. L. Jiang, J. Caggiano, J. P. Greene, A. Heinz, D. Henderson, R. V. F. Janssens, E. F. Moore, G. Mukherjee *et al.*, Phys. Rev. C **67**, 065809 (2003).
[19] D. W. Visser, J. A. Caggiano, R. Lewis, W. B. Handler, A. Parikh, and P. D. Parker, Phys. Rev. C **69**, 048801 (2004).
[20] W. P. Tan, J. Görres, J. Daly, M. Couder, A. Couture, H. Y. Lee, E. Stech, E. Strandberg, C. Ugalde, and M. Wiescher, Phys. Rev. C **72**, 041302(R) (2005).
[21] C. E. Rolfs and W. S. Rodney, *Cauldrons in the Cosmos* (University of Chicago, Chicago, 1988).
[22] R. Kanungo, T. Alexander, A. Andreyev, G. Ball, R. Chakrawarthy, M. Chicoine, R. Churchman, B. Davids, J. Forster, S. Gujrathi *et al.*, Phys. Rev. C **74**, 045803 (2006).
[23] S. Mythili, B. Davids, T. K. Alexander, G. C. Ball, M. Chicoine, R. S. Chakrawarthy, R. Churchman, J. S. Forster, S. Gujrathi, G. Hackman *et al.*, Phys. Rev. C **77**, 035803 (2008).
[24] F. de Oliveira, A. Coc, P. Aguer, C. Angulo, G. Bogaert, J. Kiener, A. Lefebvre, V. Tatischeff, J. P. Thibaud, S. Fortier *et al.*, Nucl. Phys. **A597**, 231 (1996).
[25] M. Kurokawa, K. I. Hahn, P. Strasser, S. Kubono, T. Koike, X. Liu, T. Miyachi, Y. Fuchi, S. C. Jeong, H. Kawashima *et al.*, in *International Symposium on Origin of Matter and Evolution of Galaxies 97 : Atami, Japan, 5–7 November 1997*, edited by S. Kubono, T. Kajino, K. I. Nomoto, and I. Tanihata (World Scientific, Singapore, 1998), p. 245.

[26] H. T. Fortune, H. Nann, and B. H. Wildenthal, Phys. Rev. C **18**, 1563 (1978).
[27] F. Becchetti, M. Lee, T. O'Donnell, D. Roberts, J. Kolata, L. Lamm, G. Rogachev, V. Guimares, P. DeYoung, and S. Vincent, Nucl. Instrum. Methods A **505**, 377 (2003).
[28] G. R. Satchler, *Introduction to Nuclear Reactions* (Wiley, New York, 1980).
[29] T. Motobayashi (private communication).
[30] H. T. Fortune and R. Sherr, Phys. Rev. C **73**, 024302 (2006).
[31] D. Tilley, H. Weller, C. Cheves, and R. Chasteler, Nucl. Phys. **A595**, 1 (1995).
[32] H. T. Fortune and A. G. Lacaze, Phys. Rev. C **67**, 064305 (2003).
[33] S. Wilmes, V. Wilmes, G. Staudt, P. Mohr, and J. W. Hammer, Phys. Rev. C **66**, 065802 (2002).
[34] Á. Z. Kiss, B. Nyakó, and E. Somorjai, Nucl. Instrum. Methods Phys. Res. **203**, 107 (1982).
[35] P. V. Magnus, M. S. Smith, P. D. Parker, R. E. Azuma, C. Campbell, J. D. King, and J. Vise, Nucl. Phys. **A470**, 206 (1987).
[36] D. Rogers, J. Aitken, and A. Litherland, Can. J. Phys. **50**, 268 (1972).
[37] J. Aitken, R. Azuma, A. Litherland, A. Charlesworth, D. Rogers, and J. Simpson, Can. J. Phys. **48**, 1617 (1970).
[38] D. M. Pringle and W. J. Vermeer, Nucl. Phys. **A499**, 117 (1989).
[39] J. Davidson and M. Roush, Nucl. Phys. **A213**, 332 (1973).
[40] S. Utku, J. G. Ross, N. P. T. Bateman, D. W. Bardayan, A. A. Chen, J. Görres, A. J. Howard, C. Iliadis, P. D. Parker, M. S. Smith *et al.*, Phys. Rev. C **57**, 2731 (1998).
[41] M. Dufour and P. Descouvemont, Nucl. Phys. **A672**, 153 (2000).
[42] J. L. Fisker, W. Tan, J. Görres, M. Wiescher, and R. L. Cooper, Astrophys. J. **665**, 637 (2007).